Excited-State Symmetry Breaking in an Aza-nanographene Dye

FULL PAPER

Excited-State Symmetry Breaking in an Aza-nanographene Dye

Brunella Bardi,[a] Maciej Krzeszewski,[b] Daniel T. Gryko,*[b] Anna Painelli,[a] and Francesca Terenziani*[a]

Abstract: The photophysics of a structurally unique aza-analogue of polycyclic aromatic hydrocarbons characterized by 12 conjugated rings and a curved architecture is studied in detail. The combined experimental and computational investigation reveals that the lowest excited state has charge-transfer character in spite of the absence of any peripheral electron-withdrawing groups. The exceptionally electron-rich core comprised of two fused pyrrole rings is responsible for it. The observed strong solvatofluorochromism is related to symmetry breaking occurring in the emitting excited state, leading to a significant dipole moment (13.5 D) in the relaxed excited state. The anomalously small fluorescence anisotropy of this molecule, qualitatively different from what is observed in standard quadrupolar dyes, is explained as due to the presence of excited states being close in energy but having different polarization directions.

Introduction

Pyrrolo[3,2-*b*]pyrroles have recently been reported as extremely interesting materials for molecular electronics, photonics and photovoltaics.[1,2] Despite their young age, these dyes have already been applied in research related to organic light-emitting diodes,[3] resistive memory devices,[4] bulk heterojunction organic solar cells,[5] aggregation-induced emission,[6] photochromic analysis of halocarbons,[7] MOFs,[8] and dye-sensitized solar cells.[9] Their electronic absorption spectra are insensitive to solvent polarity, in line with a centrosymmetric structure. On the opposite, their fluorescence spectra show a pronounced solvatochromism, despite the absence of electron-donating/ withdrawing groups in the periphery of these structures.

Solvatofluorochromism in centrosymmetric structures is typical of so-called quadrupolar chromophores, which consist of a D-π-A-π-D (or A-π-D-π-A) network of electron donating (D) and electron withdrawing (A) groups linked through π-conjugated bridges. Their low-energy spectroscopic behavior is governed by intramolecular charge-transfer (CT) phenomena, promoting intense and tunable absorption in the visible range, good electron transport properties and large nonlinear optical responses.[10–12]

The highly symmetric structure of quadrupolar chromophores implies negligible permanent dipole moments in the ground state and non-polar vertical excited states. However, positive solvatochromic shifts in emission have been reported for many quadrupolar dyes, indicating the existence of a polar emissive state.[13–19] Recently, symmetry breaking effects leading to an asymmetrical distribution of the electronic excitation on the two molecular arms has been monitored in real time through transient spectroscopy.[20–27]

Solvatochromic effects in quadrupolar chromophores were naturally rationalized by essential-state models, as related to charge instabilities of either the ground or the excited state.[28] In chromophores with weak D and A groups (class I chromophores), where the ground state has a small degree of charge transfer, i.e. the quadrupolar moment is small, the first excited state is bistable: the vertical excited state reached upon absorption, characterized by a symmetric charge distribution, relaxes in a broken-symmetry structure, conferring a dipolar character to the relaxed excited state responsible for fluorescence.

The pyrrolo[3,2-*b*]pyrrole (PP), being an electron rich heterocyclic unit,[1,29,30] behaves as an energy donor moiety in A-π-D-π-A-type chromophores, when coupled to strong electron withdrawing moieties like cyano,[23,24] nitro[31,32] and carbonyl groups.[33] PP-derivative **1** (Figure 1) has a qualitatively different structure from previously investigated PP-based quadrupolar dyes. Its butterfly-shaped architecture is obtained via the expansion of the π-structure of the PP core with large peripheral 'wings', for a total of 12 fused aromatic rings. Steric hindrance between the hydrogen atoms on opposite sides of the wings prevents this system from planarity, forcing it in a double helical conformation.[2] Two conformational isomers of **1** were found in the crystalline phase: a folded *meso* diastereoisomer (belonging to the C_i point group) and a helical twisted form of C_2 symmetry, existing in the (*P*,*P*) and (*M*,*M*) enantiomers (Figure 1, right). The isomers could not be distinguished in solution because of low interconversion energy barrier (56.0 kJ mol^{-1}) and fast interconversion rate.[2]

The solvatochromic behaviour of fluorescence spectra of **1** suggests the occurrence of excited-state symmetry breaking, as typical of class I quadrupolar dyes.[28] The observation of the behaviour typical of class I quadrupolar dyes in a system with a markedly different architecture, lacking well-identified A groups, inspired further experimental and theoretical investigation of **1**. Interestingly, we found that its fluorescence anisotropy significantly differs from what is commonly observed in quadrupolar dyes, pointing to a more complex electronic structure. A detailed TDDFT study allowed us rationalize the results and

[a] B. Bardi, Prof. A. Painelli, Prof. F. Terenziani
Department of Chemistry, Life Sciences and Environmental Sustainability, University of Parma, Parco Area delle Scienze 17/a, 43124 Parma, Italy
E-mail: francesca.terenziani@unipr.it
[b] Dr. M. Krzeszewski, Prof. D. T. Gryko
Institute of Organic Chemistry, Polish Academy of Sciences
Kasprzaka 44-52, 01-224 Warsaw, Poland
E-mail: dtryko@icho.edu.pl

Supporting information for this article is given via a link at the end of the document.

unravel the quadrupolar nature of the chromophore. Based on these data, we then addressed essential-state modelling of **1** as a A-π-D-π-A quadrupolar dye, further supporting this hypothesis.

With the growing number of unprecedented curved aza-nanographenes published within the last 5 years,[34–36] this study offers both general understanding of their optical behaviour and guidelines for design of solvatofluorochromic dyes possessing large fluorescence quantum yield across the solvent polarity scale.

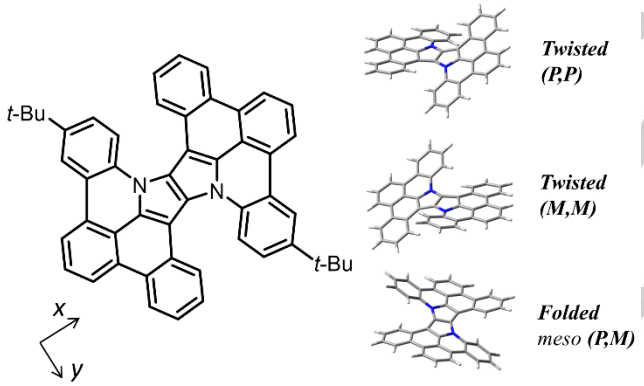

Figure 1. Molecular structure of **1** (left) and sketch of its conformational isomers (right, for clarity *t*-butyl groups are substituted with hydrogen atoms).

Results and Discussion

Spectroscopic data

Absorption of **1** occurs over a broad spectral range in the UV region, with a less intense band in the blue, and is barely affected by solvent polarity. The oscillator strength associated to the lowest-energy absorption band amounts to ~0.3, corresponding to a transition dipole moment of ~6 D. The emission band is largely solvatochromic, and redshifts from 451 nm in cyclohexane to 505 nm in dimethyl sulfoxide (DMSO). The fluorescence quantum yield increases from 17% to 32% from toluene to DMSO, with lifetimes ranging from 16.8 to 18.9 ns.[2] From the Weisskopf-Wigner equation for the radiative decay rate,[37,38] the transition dipole moment associated with emission is estimated to amount to ~3 D, quite independently of the solvent. This transition dipole moment, considerably smaller than the transition dipole moment estimated for the lowest energy absorption band, gives a first hint about the non-correspondence of the absorbing and emitting states.

To better investigate this intriguing phenomenon, as well as the origin of the quadrupolar-like emission solvatochromism of dye **1**, we measured its fluorescence anisotropy, retrieving information on the polarization of the excited states accessed in absorption relative to the polarization of the emissive excited state.

Upon excitation with polarized light, the emission from many samples is in turn polarized. The extent of polarization of the emission is measured as anisotropy.[39] Typically, the sample is irradiated with linearly polarized light and the intensity of the emitted light is detected through a polarizer oriented in the same direction as the excitation light ($I_{\parallel}$) and in the perpendicular direction ($I_{\perp}$). Fluorescence anisotropy r is defined as:[39,40]

$$r = \frac{I_{\parallel} - I_{\perp}}{I_{\parallel} + 2I_{\perp}} \quad (1)$$

For randomly distributed molecules in solution, the maximum anisotropy value that can be obtained is the so-called fundamental anisotropy r_0, that is related to the angle α between the absorption and the emission dipole moments of the fluorophore:[39,40]

$$r_0 = \frac{2}{5}\left(\frac{3\cos^2\alpha - 1}{2}\right) \quad (2)$$

In absence of trivial depolarization effects, such as rotation of the fluorophore during the excited-state lifetime, the measured r value is close to r_0, offering the possibility to estimate the relative orientation of the transition dipole moments of absorption and fluorescence transitions.

In this work, fluorescence anisotropy of **1** was measured in undercooled solvents of different polarity, namely non-polar methylcyclohexane (MeChx) and mildly polar 2-methyltetrahydrofuran (2-MeTHF), as well as in a viscous solvent (polytetrahydrofuran, pTHF) at room temperature (Figure 2). In all cases, the rotational motion of the solute is slow compared to fluorescence lifetime, preventing rotational depolarization, thus ensuring $r = r_0$. Liquid and glassy solvents behave in a different way: the solvation sphere formed by a liquid solvent readjusts in response to the solute excitation, while in glassy solvents it is blocked in the configuration equilibrated with the ground-state solute.

Fluorescence excitation spectra of **1** in Figure 2 nicely match absorption spectra,[2] showing two groups of closely spaced signals, one in the 300-350 nm region, with a sharp peak at ~350 nm, and another beyond 400 nm, with a maximum at ~430 nm. Vibronically resolved emission spectra are obtained in frozen solvents with maximum intensity at 450 nm. In polar pTHF solvent the vibronic structure is smeared out as a result of inhomogeneous broadening.

Excitation anisotropy (i.e. anisotropy measured at fixed emission wavelength while scanning on the excitation wavelength) smoothly increases from 0 for excitation at ~430 nm to ~0.1 at ~300 nm, following the same trend in all the experimental conditions. In glassy solvents, when detecting at the emission wavelength of the 0-0 vibronic line (450 nm), r spans a large range of values between -0.1 and 0.2 in MeChx and 2-MeTHF (red symbols in Figure 2). For excitation wavelength > 430 nm, anisotropy increases abruptly approaching ~0.25 at the limit of the experimental window, corresponding to a weak tail in the excitation spectrum, that overlaps with the emission band. Similar results, with *r* approaching large values in the λ > 430 nm region, are consistently obtained also upon detection at different emission wavelength.

These data can be interpreted as follows. Vertical excitation brings the molecule to one of its optically allowed excited states. The absorption transition dipole moment depends on the state

reached upon excitation, which is dictated by the wavelength of the incoming light and by selection rules. From the vertical excited state, population relaxes on a sub-picosecond timescale towards the lowest excited state through internal conversion (Kasha rule) before radiative emission. Because of fast internal conversion, the emissive state is always the lowest-lying excited state (S_1), therefore the emission dipole moment is the same, irrespectively of the excitation wavelength. When the system is directly excited to the first excited state S_1, absorption and emission involve the very same state, and we expect α = 0, and hence, according to Eq. 2, r = 0.4. This trivial result is common to most of the chromophores: excitation anisotropy amounts to ~0.4 in the excitation wavelength region corresponding to the $S_0 \rightarrow S_1$ transition. In this respect, the behaviour of **1** is anomalous. The excitation anisotropy is in fact close to zero at the frequency of the maximum of the lowest-energy absorption band (~430 nm), suggesting an angle α close to the magic angle 54.7°. This value indicates that the excited state responsible for the lowest-energy absorption band with a sizable intensity is not the same state responsible for emission. The sharp rise of r in the red edge of the excitation spectrum suggests instead that another lower-lying excited state is present in this region, characterized by a different polarization (α ~ 30° or an angle with the same squared cosine) and a much lower oscillator strength. Moreover, in glassy solvents, where solvent relaxation is hampered, the emission spectrum overlaps with the long-wavelength absorption tail. We therefore conclude that S_1 state, i.e. the state responsible for emission, is a weakly absorbing state located in the red tail of the lowest-energy absorption band. Computational studies described in the following section fully support this hypothesis.

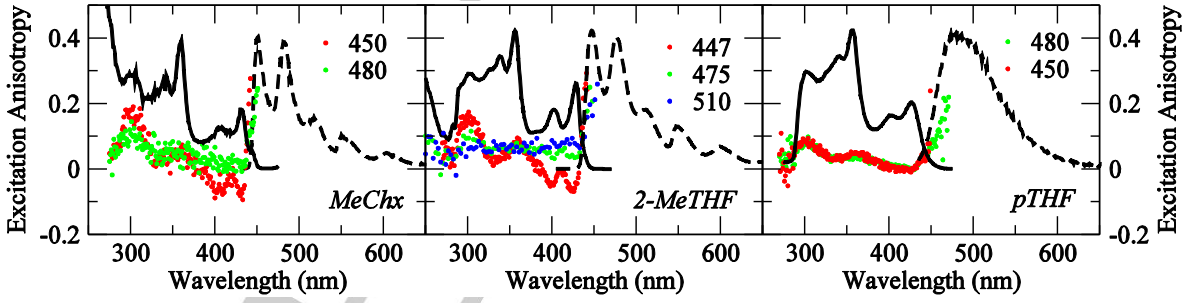

Figure 2. Fluorescence excitation anisotropy (dots) of **1** in different solvents: glassy methylcyclohexane (MeChx) at 77 K, glassy 2-methyltetrahydrofuran (2-MeTHF) at 77 K and liquid polytetrahydrofuran (pTHF) at room temperature. Anisotropies were collected detecting at different emission wavelengths, reported in the legends (in nm). Excitation and emission spectra collected under the same experimental conditions (continuous and dashed lines, respectively) are reported to guide the eye.

Table 1. TDDFT results on **1** obtained in gas phase and DMSO at B3LYP/6-31+G(d,p) level. Transition energies *E*, transition wavelengths λ, oscillator strengths *f*, squared transition dipole moments μ^2 and their components (referring to the Cartesian axes in Figure 1), main excitations involved. For the first three excited states, energies in italic were computed with state-specific corrections.

		***E* (eV)**	**λ (nm)**	***f***	**μ_x (D)**	**μ_y (D)**	**μ_z (D)**	**μ^2 (D²)**	**Type (>20%)**
Gasphase	S_1	2.841	436.4	0.0065	-	-	0.778	0.606	H→L+1 (98%)
	S_2	2.843	436.1	0.0546	-0.244	-2.236	-	5.058	H→L (87%)
	S_3	3.000	413.4	0.2508	-4.422	1.572	-	22.021	H→L+2 (79%)
	S_4	3.393	365.4	0.0017	-	-	0.359	0.129	H-1→L+1 (82%)
	S_5	3.465	357.9	0.3744	-5.324	-0.339	-	28.456	H-1→L (79%)
DMSO	S_1	2.871 *2.673*	431.9 *463.8*	0.0094	-	-	-0.928	0.861	H→L+1 (98%)
	S_2	2.872 *2.673*	431.6 *463.8*	0.0921	-0.385	-2.881	-	8.445	H→L (84%)
	S_3	2.974 *3.010*	416.8 *411.9*	0.4101	-5.687	1.990	-	36.306	H→L+2 (78%)
	S_4	3.412	363.4	0.0026	-	-	0.451	0.204	H-1→L+1 (79%)
	S_5	3.457	358.6	0.5466	6.379	0.966	-	41.628	H-1→L (84%)

TDDFT results

We exploit density functional theory (DFT) and its time-dependent (TDDFT) extension[41–44] to explore ground and excited-state properties of **1**. Polar solvation cooperates with symmetry breaking in stabilizing the relaxed dipolar state,[28] therefore implementation of solvation effects is fundamental to rationalize spectral properties. We adopt an implicit treatment of the solvent as provided by the Polarizable Continuum Model (PCM).[45–47] To stress the effect of polar solvation, we present results obtained in dimethyl sulfoxide (DMSO), a strongly polar solvent (ε_{DMSO} = 46.7).

DFT geometry optimizations were performed on the two conformational isomers of **1** (twisted and folded) recognized in crystallographic studies, adopting Becke, 3-parameters, Lee-Yang-Parr hybrid functional (B3LYP)[48] and 6-31+G(d,p) basis set. To reduce the computational cost, *t*-butyl groups were substituted with hydrogen atoms, with marginal effects on calculated spectral properties. The folded form was found to be less stable than the twisted form, the energy difference between the conformers amounting to 9.9 kJ mol^{-1} in DMSO, in agreement with previously published data.[2] Accordingly, at equilibrium, the twisted form is largely favoured over the folded form and dominates the spectroscopic behaviour of **1**. Therefore, in the following we will just discuss the twisted enantiomer, namely the (*P*,*P*) form. For the sake of completeness, results on the folded form are provided as Supporting Information.

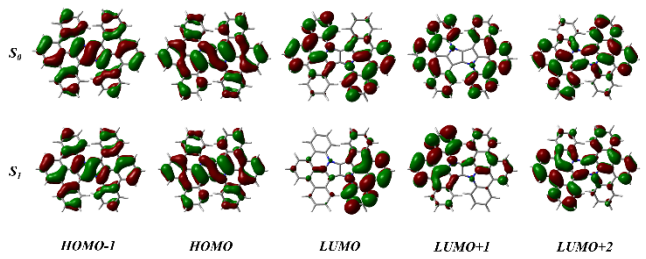

Figure 3. Frontier molecular orbitals of **1** in the ground state geometry (top) and S_1 optimized geometry (bottom) computed in DMSO at B3LYP/6-31+G(d,p) level (isovalue of the contour plots: 0.02).

TDDFT results for the five lowest-energy electronic transitions of **1** are collected in Table 1. Two transitions with high oscillator strength are found in the gas phase, $S_0 \rightarrow S_3$ and $S_0 \rightarrow S_5$, located at 413.4 nm (3.0 eV) and 357.9 nm (3.4 eV), respectively. Two closely spaced weakly allowed transitions are found at lower energy, ~436 nm (2.8 eV), one polarized along the C_2 molecular axis and the other lying in the perpendicular *xy* plane.

Analogous results were obtained in DMSO, where the $S_0 \rightarrow S_3$ and $S_0 \rightarrow S_5$ transitions (416.8 and 358.6 nm, respectively) have large oscillator strengths, while low-lying $S_0 \rightarrow S_1$ and $S_0 \rightarrow S_2$ transitions (~432 nm) have much lower oscillator strengths. Inspection of the molecular orbitals involved in the transitions (Figure 3, top) offers a visualization of the molecular substructures involved in the excitation process. Occupied orbitals HOMO and HOMO-1 extend over the entire conjugated backbone, with sizable electronic density residing on the PP core. LUMO is mainly localized in the molecular wings, only marginally involving the PP rings. LUMO+1 extends at the periphery of the expanded structure only, with nodes in the central region. $S_0 \rightarrow S_1$ has an almost pure HOMO→LUMO+1 character, and $S_0 \rightarrow S_2$ coincides with the HOMO→LUMO transition. In both cases, the excitation implies a charge migration from the molecular core to the peripheral wings, suggesting a partial CT character. On the opposite, $S_0 \rightarrow S_3$, mainly a HOMO→LUMO+2, involves a charge redistribution over the entire molecule and has not an explicit CT character. Energies of $S_0 \rightarrow S_1$ and $S_0 \rightarrow S_2$ are red-shifted by ~32 nm (0.2 eV) when adopting the state-specific solvation approach,[49] in agreement with their CT nature. The energy of $S_0 \rightarrow S_3$ is instead barely affected by state-specific solvation, as typical for localized transitions.

The description of excited states of **1** offered by TDDFT agrees well with experimental data. Specifically, $S_0 \rightarrow S_3$ matches with the experimental absorption at 427 nm (with an error less than 0.1 eV), while $S_0 \rightarrow S_5$ compares well with the intense experimental absorption peak at 360 nm. The fact that other electronic transitions are found below $S_0 \rightarrow S_3$ suggests that emission comes from a lower-energy CT state (either S_1 or S_2), whose absorption, with lower intensity, overlaps the red-edge tail of the $S_0 \rightarrow S_3$ peak. This is consistent with the apparent Stokes shift observed in frozen solvents.

Failure of B3LYP functional in the description of CT states is however a well-known problem. Specifically, low-lying dark CT states are sometimes obtained as an artefact of the functional.[50,51] Therefore we repeated the calculations in DMSO using the hybrid exchange-correlation functional CAM-B3LYP.[52] Relevant results are reported as Supporting Information (Table S1). CAM-B3LYP performs much worse than B3LYP: main transitions are predicted at 363 nm (3.41 eV) and 309 nm (4.02 eV), i.e. blue-shifted from experiment with an error amounting to more than 65 nm (0.5 eV) for the first absorption band and 50 nm (0.6 eV) for the second band. When accounting for state-specific corrections, the three lowest-energy transitions are close in energy (within 0.15 eV or less according to state-specific), stressing that in this spectral region the spectroscopy of **1** is governed by the interplay between these three transitions, in agreement with B3LYP results. For these reasons, in the following we limit our analysis to B3LYP results.

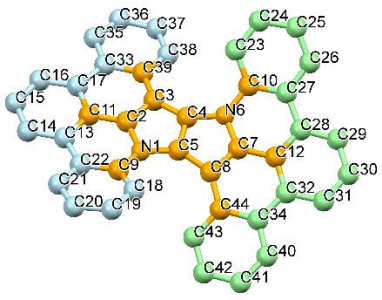

Figure 4. Geometry of **1** in the relaxed S_1 state (H atoms omitted) with the atom numbering used in the definition of geometrical parameters in Table 2 and the colour code for the definition of the regions in Table 3: left (light blue), centre (orange), right (green).

The first excited state of **1** was optimized in DMSO. The S_1 minimum was found 255.0 kJ mol^{-1} (2.64 eV) higher than the ground state, with the geometry sketched in Figure 4. Bond lengths and angles are not significantly affected by relaxation. Indeed, the main geometrical distortions involve the deformation of the molecular core, with effects on the dihedral angles, especially in the junction region between the PP core and the lateral wings (Table 2). Variations of the dihedrals up to 6.5° were found. These variations are small, nonetheless they are significant, particularly in view of the fused and hence intrinsically rigid structure of the molecule of interest. At the S_1 minimum, dihedral angles are no more equivalent by C_2 rotation, suggesting a broken-symmetry structure. Prominent effects of symmetry breaking are indeed found on molecular orbitals (Figure 3, bottom). While occupied orbitals are basically the same as for the ground state, LUMO and LUMO+1 are strongly distorted in S_1, and are distributed mostly on one of the two wings. Thus, upon relaxation, the excitation localizes on one of the two molecular wings, and C_2-symmetry is broken. This has a large impact on the dipole moment of the molecule. According to our calculations, **1** in the ground state has a residual permanent dipole moment of 0.79 D aligned along the C_2 axis (*z*), that becomes 0.61 D in the vertical (unrelaxed) S_1 state. In the relaxed broken-symmetry S_1 state, the molecular dipole moment becomes fairly large (13.5 D), with sizable components in the *xy* plane. This highly dipolar state is stabilized in polar solvents, explaining the observed large and positive solvatochromism of fluorescence.

Table 2. Geometrical parameters (dihedral angles involving atoms of the PP core) of **1** computed in DMSO (B3LYP/6-31+G(d,p)) in the ground state S_0 and the first excited state S_1 optimized structures. Dihedrals are grouped in pairs for equivalency by rotation around the C_2 axis.

dihedral	S_0 (°)	S_1 (°)
N1-C5-C8-C44 N6-C4-C3-C39	7.09 7.09	1.59 0.92
C9-N1-C5-C8 C10-N6-C4-C3	35.65 35.65	40.91 39.74
C2-N1-C5-C8 C7-N6-C4-C3	-162.64 -162.64	-156.80 -156.21
C18-C9-N1-C5 C23-C10-N6-C4	2.36 2.36	1.88 1.71
C5-C8-C44-C43 C4-C3-C39-C38	2.89 2.89	5.64 6.79
N1-C5-C4-N6	177.56	178.85
C3-C4-C5-C8	163.77	158.51

To gain more information on the nature of the states, we partitioned the molecule in three regions, corresponding to the PP core and to the two wings, as shown in Figure 4. While this partitioning is somewhat arbitrary, the charge distribution in the three fragments, reported in Table 3, is interesting. In the ground state (1st column) a small positive charge resides on the PP, being a weak electron donor, while the balancing negative charge is equally shared by the molecular wings. Upon vertical excitation to S_1 (2nd column), the charge on the central PP becomes more positive, and the charge on the left and right wings becomes more negative, indicating a symmetrical CT from the centre to the peripheral regions of the molecule. For the relaxed geometry relevant to S_1 (3rd and 4th columns), we find an asymmetric charge distribution over the molecule: for the excited state S_1, the charges residing on the left and right wings are very different, signalling symmetry breaking in the relaxed excited state.

We conclude that, in spite of its structure with π-conjugation extending in 2D, **1** behaves like a quadrupolar chromophore with a broken-symmetry relaxed excited state. A basic A-π-D-π-A structure can be recognized as well, where the PP plays the role of the electron donor and the expanded wings act as electron acceptors.

Emission of **1** in DMSO is predicted at 511.6 nm (2.42 eV) with linear response solvation, and compares well with experimental data (505 nm, 2.45 eV), whereas state-specific solvation locates emission at higher energy (2.65 eV, 468 nm). Emission involves mainly a HOMO←LUMO transition (98%) and has a significant oscillator strength (0.167), suggesting that fluorescence is an allowed process, in agreement with the measured high quantum yield. The corresponding transition dipole moment amounts to 4 D, in very good agreement with the 3 D estimate obtained above from the experimental values of the fluorescence quantum yield lifetime.

Table 3. Charge distribution of **1** obtained from Hirshfeld charge analysis[53]. Regions are defined according to the colour code in Figure 4.

	S_0 geometry		**S_1 geometry**	
	S_0	**S_1**	**S_0**	**S_1**
centre	0.0361	0.1883	0.0327	0.1930
left	-0.0180	-0.0941	-0.0120	-0.3962
right	-0.0180	-0.0941	-0.0206	0.2032

To address excitation anisotropy we focused attention on the three electronic states responsible for the low-energy absorption features (Figure 5). According to the Kasha rule, we assume that emission always occurs from the S_1 relaxed state. Absorption from S_0 to S_1 is polarized along the C_2 axis, while emission from relaxed S_1 to S_0, thanks to the helical nature of the chromophore and symmetry breaking effects, is almost aligned with one molecular wing. The resulting angle between the corresponding transition dipoles amounts to approximately 77°, that according to eq. 2 corresponds to a negative anisotropy (r ~ -0.17). The transition dipole for the $S_0 \rightarrow S_2$ transition forms an angle of about 28° with the emission dipole, giving a large and positive r (0.27). Finally, the angle between emission and $S_0 \rightarrow S_3$ dipole moments is about 126°, yielding an anisotropy value close to zero.
These results compare well with experimental data. Indeed anisotropy is an additive quantity, so that the measured anisotropy at any wavelength, $r(\lambda)$, is given by:

$$r(\lambda) = \sum_{i=1}^{N} f_i(\lambda) r_i \quad (3)$$

where $f_i(\lambda)$ is the fractional contribution of the *i*-th transition to the total absorption at λ, r_i is the corresponding limiting anisotropy and the sum is extended over the *N* excited states of the fluorophore.[39]

In order to quantitatively apply eq. (3), the absorption spectrum has to be known. First principle calculation of the vibronic structure of the absorption spectra of **1** is beyond the aim of the present work, however we can make some interesting considerations. The three transitions considered in Figure 5 are confined in a very narrow (< 0.2 eV wide) spectral window, therefore we expect that homogeneous and inhomogeneous broadening effects lead to a strong overlap of the corresponding bands, each one contributing to the total intensity with a different weight, proportional to the oscillator strength. The absorption band at ~430 nm has a large contribution from the $S_0 \rightarrow S_3$ transition, therefore we expect *r* ~ 0.006 in proximity of the maximum of the absorption spectrum. $S_0 \rightarrow S_2$ lies at lower energy, forming a weak tail in the red-side of the absorption band, where the contribution of the $S_0 \rightarrow S_3$ transition drops down: the anisotropy is expected to increase abruptly to the value relevant to the S_2 state (*r* > 0.2). The $S_0 \rightarrow S_1$ transition is expected nearby, with a negative *r*, however its oscillator strength is too low to give an appreciable contribution.

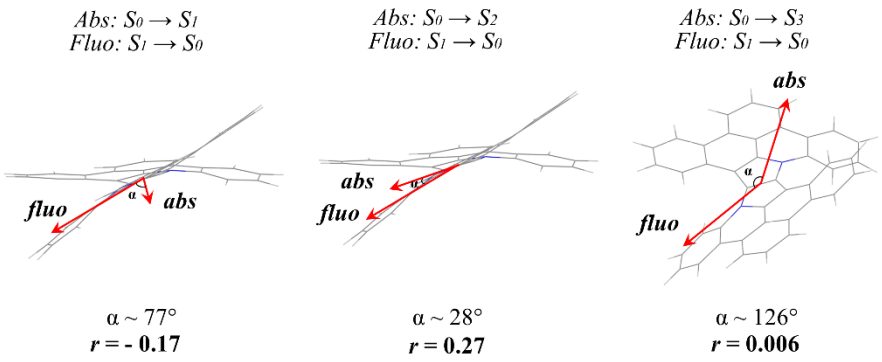

Figure 5. Absorption and emission dipole moments (represented for convenience as vectors) of **1** computed in DMSO at B3LYP/6-31+G(d,p) level. Emission is assumed always from S_1, while absorption has been considered for the three lowest transitions. The calculated angle α between absorption and emission dipole moments and the expected value of anisotropy *r* are shown on the panels.

Essential-State modelling

Essential-state models (ESMs) provide a simple and physically sound description of CT chromophores[54–56] and their aggregates,[57–61] and were effective in rationalizing the different propensity to symmetry breaking of various families of quadrupolar and octupolar dyes.[28,62,63] ESMs describe each dye in terms of a minimal set of basis states, corresponding to the main resonating structures. The complex absorption spectrum of **1**, with at least three electronic states responsible for the observed visible spectrum, is well beyond any few-state model and we will not attempt to reproduce it in detail. However, taking TDDFT results as a reference, we define a minimal model for **1**, described as a A-π-D-π-A dye.

Three resonating structures, DAD, D^+A^-D and DA^-D^+ (see also Fig. 6), represent the minimum basis for quadrupolar dyes.[28] Two parameters enter the Hamiltonian, $2z$, measuring the energy difference between the neutral DAD and the two degenerate zwitterionic states, D^+A^-D and DA^-D^+, and $-\sqrt{2}t$, quantifying the probability of electron transfer from the donor to either one of the two acceptor sites. Accounting for symmetry, the two degenerate zwitterionic states are combined in a symmetric, $|Z_+\rangle$, and an antisymmetric combination, $|Z_-\rangle$. The symmetric states $|N\rangle$ and $|Z_+\rangle$ are mixed to give the ground state $|g\rangle$ and the second excited state $|e\rangle$. The first excited state, $|c\rangle$, coincides with $|Z_-\rangle$. Thus, we expect two CT transitions, $|g\rangle \rightarrow |c\rangle$ and $|g\rangle \rightarrow |e\rangle$, with energies E_{gc} and E_{ge} respectively. For linear systems, as depicted in Figure 6, strict selection rules apply and only the $|g\rangle \rightarrow |c\rangle$ transition is allowed in absorption. Transition energies are:[28]

$$E_{gc} = 2t\sqrt{\frac{1-\rho}{\rho}} \quad (4)$$

$$E_{ge} = 2t\sqrt{\frac{1}{\rho(1-\rho)}} \quad (5)$$

where ρ measures the weight of $|Z_+\rangle$ in the ground state, and hence the quadrupolar character of the chromophore. It is related to model parameters as follows:

$$\rho = \frac{1}{2}\left(1 - \frac{z}{\sqrt{z^2+4t^2}}\right) \quad (6)$$

The electronic model can be extended to include intramolecular vibrations,[28,64] allowing to address symmetry breaking and vibronic effects. Two mutually decoupled effective vibrational coordinates with harmonic frequency ω_v and vibrational relaxation energy ε_v are introduced to account for nuclear relaxation along each molecular arm. These coordinates can be symmetry adapted in a totally-symmetric (Q_+) and an antisymmetric (Q_-) vibration, the last one being the coordinate

accounting for symmetry breaking effects. In particular, quadrupolar dyes can be classified according to the ρ value.[28,63] Chromophores with low quadrupolar moment ($\rho < \sim 0.2$) belong to class I: they have a stable ground state and are prone to symmetry breaking in the first excited state. For large ρ ($\rho \to 1$), we have typical class III chromophores, where symmetry breaking affects the ground state. For intermediate ρ (class II) no charge instabilities are expected, and all states are non-dipolar.

Dye **1** has a large conjugated structure and in the twisted form it lacks the inversion centre. Accordingly, several electronic states with different polarization directions are accessible upon visible light absorption. Our TDDFT analysis suggests that $S_0 \rightarrow S_1$ and $S_0 \rightarrow S_2$, have a CT character, making these states suitable for an ESM description.

The TDDFT energies of $S_0 \rightarrow S_1$ and $S_0 \rightarrow S_2$ (gas phase values) give an estimate for E_{gc} and E_{ge}, respectively. $|c\rangle$ and $|e\rangle$ states (corresponding to S_1 and S_2) are very close in energy, suggesting a small mixing between $|N\rangle$ and $|Z_+\rangle$, i.e. a small t value. Indeed, eqn. (4) and (5) yield t = 0.03 eV and $\rho \sim 6 \cdot 10^{-4}$, safely locating **1** in class I. The symmetry-allowed *g*→*c* transition is expected to have very low intensity, being proportional to ρ.

The parameters ω_v and ε_v were extracted from experimental emission spectra. Specifically, ω_v was set to reproduce the vibrational spacing observed in cyclohexane, while ε_v allowed to reproduce the vibronic progression. Spectra are obtained assigning to each transition a Gaussian shape with half-width at half maximum γ.

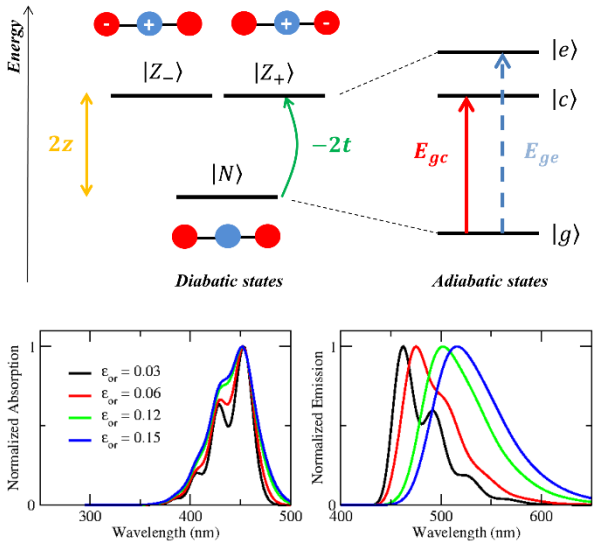

Figure 6. Essential-state modelling of **1**. Top: the three-state model for a quadrupolar A-π-D-π-A chromophore. Sketch of the diabatic states (left) (blue: electron donor, red: electron acceptor) and adiabatic states (right). Bottom: calculated CT absorption (left) and emission (right) spectra of **1** in solvents of different polarity. Parameters are given in Table 4, ε_{or} reported in the legend (in eV) is adjusted to reproduce emission spectra in various solvents reported in Ref[2] (black: cyclohexane, red: toluene, green: tetrahydrofuran, blue: dimethylsulfoxide).

Table 4. Model parameters for **1**.

z (eV)	$\sqrt{2}t$ (eV)	ω_v (eV)	ε_v (eV)	γ (eV)
1.42	0.04	0.16	0.10	0.05

In polar solvents, additional effects arise from the interaction between the electronic degrees of freedom of the solute and the slow orientational motion of the solvent molecules.[65] These effects are introduced in the model in a reaction field approach, where the solvent is treated as a continuum dielectric medium.[28,54,55,66] A single solvent-dependent parameter related to the solvent restoring force, the solvation relaxation energy ε_{or}, accounts for solvent polarity, while all other model parameters are solvent-independent and are kept fixed.

Spectra of **1** in solution, only relevant to the CT transitions (Figure 6, bottom), were calculated with the parameter set reported in Table 4. The absorption maximum is not affected by the solvent polarity and only inhomogeneous broadening effects take place in polar solvents. Direct comparison of experimental and calculated absorption spectra is hindered by the fact that the $|g\rangle \rightarrow |c\rangle$ transition overlaps with the much more intense $S_0 \rightarrow S_3$ not included in the ESM. The transition dipole moment associated to this transition is expected to be extremely small if compared to the transition dipole of $S_0 \rightarrow S_3$. The comparison between experimental and calculated emission spectra is instead possible and gives an impressive agreement. The emission band red-shifts with increasing solvent polarity (ε_{or}), in quantitative agreement with experiment. Moreover, the vibrational structure is well resolved in cyclohexane, while it progressively blurs upon increasing solvent polarity, in line with the experimental behaviour.

Discussion and Conclusions

In this work we explored the photophysics of a heterocyclic nanographene with butterfly shape, obtained by expanding the π-structure of the electron rich pyrrolo[3,2-*b*]pyrrole moiety. The exceptional electron-richness of this heterocyclic core induces significant charge polarization in spite of the lack of electron-withdrawing groups at the periphery. The expanded architecture as well as the curved geometry are responsible for a peculiar electronic structure, promoting interesting spectroscopic effects. Despite the highly symmetric structure, a well-pronounced emission solvatochromism is observed, typical of charge-transfer transitions, as observed in prototypical centrosymmetric quadrupolar chromophores undergoing symmetry breaking in their excited state. However, the fluorescence emission is almost depolarized upon excitation inside the lowest-energy absorption band, suggesting a much more complex excited-state scenario with respect to standard quadrupolar dyes. Another peculiar characteristic of dye **1** is the fact that its fluorescence quantum yield does not decrease in polar solvents.

Theoretical analysis unravelled the phenomena responsible for this intriguing spectroscopic behaviour, leading to a coherent rationalization of experimental data. Two complementary

theoretical frameworks, TDDFT and essential-state modelling, were adopted in a synergistic approach, revealing that, in spite of its unique structure, the target chromophore possesses an underlying quadrupolar character, where the electron rich pyrrolo[3,2-*b*]pyrrole acts as electron donor towards the weak electron withdrawing wings. The chromophore undergoes symmetry breaking in its first excited state, identifying it as a class I quadrupolar dye. On the other hand, the presence of several localized excited states lying close in energy makes the scenario more complex than in prototypical quadrupolar dyes. In fact, mainly due to the curved and twisted structure of PP, the close-lying excited states have different polarization orientations, with major effects observed in fluorescence anisotropy and in the intensity of the emission transition. Namely, the electronic transitions recognizable in the absorption spectrum are localized transitions, characterized by large oscillator strengths. The low-lying charge-transfer state is not observed in the absorption spectrum because of its very low oscillator strength. However, this very weakly allowed lowest-energy excited state is responsible for the observed fluorescence with sizable intensity. Fluorescence anisotropy measurements nicely confirm this scenario: fluorescence anisotropy is very low when exciting at the maximum of the lowest-energy absorption band (i.e. when populating a localized excited state), while it approaches the highest limiting value when exciting in the reddest tail of the absorption spectrum, where the charge-transfer state directly absorbs. The computed transition dipole moment from the relaxed charge-transfer state to the ground state is in good agreement with the one estimated from the experimental quantum yield and lifetime. In particular, this transition dipole moment is sizable (on the order of 4 D), high enough to guarantee a good fluorescence quantum yield, quite independently of the solvent. The fact that the charge-transfer transition is not recognizable in the absorption spectrum but originates an intense emission spectrum is not surprising: in the absorption spectrum, this transition is hidden underneath other more intense, close-lying localized transitions; on the other hand, fluorescence only stems from the lowest-energy excited state (in agreement with the Kasha rule), so that no competition arises. Moreover, the presence of intense localized excitations very close in energy to the charge-transfer state can induce a mixing of these types of states, the CT state borrowing intensity from the localized states.

These results open a more general perspective in the design of heterocyclic nanographenes, pointing to a complex and quite unique excited-state scenario, where a quadrupolar-like electronic structure (originating the typical solvatofluorochromism) overlaps with localized excited states characterized by different polarizations. In this respect fluorescence anisotropy is a powerful technique to identify and locate the excited states and recognizing their nature. The use of suitable and complementary theoretical tools, together with a careful spectroscopic characterization, is essential to relate the photophysical properties of complex systems to their inherent electronic structure, electron-phonon coupling and medium effects.

Experimental Section

Synthesis of **1** was reported in Ref[2]. Anisotropy measurements of **1** were performed both in undercooled solvents (methylcyclohexane and 2-methyltetrahydrofuran) and in a viscous solvent at room temperature (polytetrahydrofuran, pTHF). Anisotropy was measured on diluted (~ 10^{-6} mol L^{-1}) freshly prepared air-equilibrated solutions. All solvents were spectroscopic grade. pTHF was used as received while, to remove traces of moisture, solvents for low-temperature measurements were used after overnight storage on molecular sieves (0.3 nm) and filtered before use. Spectra and anisotropies were collected with a Fluoromax-3 Horiba Jobin-Yvon fluorometer (single channel, L-format). 2-MeTHF solutions were cooled down to 77 K at a speed of ~20 °C/min in an OptistatDN (Oxford Instruments) liquid nitrogen cryostat, using Helium as the exchange gas. MeChx solutions, contained in quartz tubes, were vitrified by direct immersion in a quartz transparent dewar filled with liquid nitrogen. This method allowed to avoid sample crystallization and to obtain clear glasses.

Computational Details

Ground state optimizations were performed at DFT level, while excited state properties were computed with is time dependent (TDDFT) extension. All calculations were performed with Gaussian16 package[67]. B3LYP and CAM-B3LYP functionals were adopted for ground state and single point TDDFT calculations, while excited state optimizations were performed with B3LYP only. Results shown were obtained with 6-31+G(d,p) basis set, including diffuse and polarization functions. Stationary points were characterized by frequency analysis. Solvation effects in DMSO were accounted for in the framework of the Polarizable Continuum Model (PCM). Optimization steps were performed adopting the standard equilibrium solvation, and transition energies were calculated with standard linear response (LR) approach, unless some cases where also state-specific (SS) corrections were computed, as implemented in Gaussian16[46,49].

Acknowledgements

The authors gratefully acknowledge financial support from the Italian Ministero dell'Istruzione, dell'Università e della Ricerca (MIUR) through the grant "Dipartimenti di Eccellenza" (DM 11/05/2017 n. 262) and from the Foundation for Polish Science (grant TEAM/2016-3/22). This project has received funding from the European Union's Horizon 2020 research and innovation programme under grant agreement No 812872 (TADFlife). This research benefits from the HPC (High Performance Computing) facility of the University of Parma, Italy.

Keywords: fused-ring systems • charge transfer • solvatochromism • polarized spectroscopy • computational chemistry

[1] M. Krzeszewski, D. Gryko, D. T. Gryko, *Acc. Chem. Res.* **2017**, *50*, 2334–2345.

[2] M. Krzeszewski, T. Kodama, E. M. Espinoza, V. I. Vullev, T. Kubo, D. T. Gryko, *Chem. - A Eur. J.* **2016**, *22*, 16478–16488.

[3] Y. Zhou, M. Zhang, J. Ye, H. Liu, K. Wang, Y. Yuan, Y. Du, C. Zhang, C. Zheng, X. Zhang, *Org. Electron.* **2019**, *65*, 110–115.

[4] R. K. Canjeevaram Balasubramanyam, R. Kumar, S. J. Ippolito, S. K.

Bhargava, S. R. Periasamy, R. Narayan, P. Basak, *J. Phys. Chem. C* **2016**, *120*, 11313–11323.

[5] R. Domìnguez, N. F. Montcada, P. de la Cruz, E. Palomares, F. Langa, *ChemPlusChem* **2017**, *82*, 1096.

[6] K. Li, Y. Liu, Y. Li, Q. Feng, H. Hou, B. Z. Tang, *Chem. Sci.* **2017**, *8*, 7258–7267.

[7] J. Wu, C.-H. Yu, J.-J. Wen, C. Chang, M. Leung, *Anal. Chem.* **2016**, *88*, 1195–1201.

[8] C. S. Hawes, G. M. Màille, K. Byrne, W. Schmitt, T. Gunnlaugsson, *Dalt. Trans.* **2018**, *47*, 10080–10092.

[9] J. Wang, Z. Chai, S. Liu, M. Fang, K. Chang, M. Han, L. Hong, H. Han, Q. Li, Z. Li, *Chem. Eur. J.* **2018**, 18032–18042.

[10] S. R. Marder, B. Kippelen, A. K. Jen, N. Peyghambarian, *Nature* **1997**, *388*, 845–851.

[11] M. Albota, D. Beljonne, J.-L. Brédas, J. E. Ehrlich, J.-Y. Fu, A. A. Heikal, S. E. Hess, T. Kogej, M. D. Levin, S. R. Marder, et al., *Science* **1998**, *281*, 1653–1656.

[12] F. Terenziani, C. Katan, E. Badaeva, S. Tretiak, M. Blanchard-Desce, *Adv. Mater.* **2008**, *20*, 4641–4678.

[13] B. Strehmel, A. M. Sarker, H. Detert, *ChemPhysChem* **2003**, *4*, 249–259.

[14] L. Ji, R. M. Edkins, L. J. Sewell, A. Beeby, A. S. Batsanov, K. Fucke, M. Drafz, J. A. K. Howard, O. Moutounet, F. Ibersiene, et al., *Chem. Eur. J.* **2014**, 13618–13635.

[15] M. Monçalves, D. da Silveira Rampon, P. E. Schneider, F. S. Rodembusch, C. da Cruz Silveira, *Dye. Pigment.* **2014**, *102*, 71–78.

[16] F. Ricci, F. Elisei, P. Foggi, A. Marrocchi, A. Spalletti, B. Carlotti, *J. Phys. Chem. C* **2016**, *120*, 23726–23739.

[17] S. A. Kurhuzenkau, M. Yezabel, C. Gomez, K. D. Bel, Y. O. Shaydyuk, D. J. Hagan, E. W. Van Stryland, C. Sissa, M. V Bondar, A. Painelli, *J. Phys. Chem. C* **2018**, *122*, 5664–5672.

[18] M. M. Raikwar, D. S. Patil, E. Mathew, M. Varghese, I. H. Joe, N. Sekar, *J. Photochem. Photobiol. A* **2019**, *373*, 45–58.

[19] B. Carlotti, A. Cesaretti, G. Cacioppa, F. Elisei, I. Odak, I. Škoric, A. Spalletti, *J. Photochem. Photobiol. A* **2019**, *368*, 190–199.

[20] N. Dozova, L. Ventelon, G. Clermont, M. Blanchard-Desce, P. Plaza, *Chem. Phys. Lett.* **2016**, *664*, 56–62.

[21] B. Dereka, E. Vauthey, *J. Phys. Chem. Lett.* **2017**, *8*, 3927–3932.

[22] J. S. Beckwith, A. Rosspeintner, G. Licari, M. Lunzer, B. Holzer, J. Fro, E. Vauthey, *J. Phys. Chem. Lett.* **2017**, *8*, 5878–5883.

[23] B. Dereka, A. Rosspeinter, R. Stezycki, C. Ruckebusch, D. T. Gryko, E. Vauthey, *J. Phys. Chem. Lett.* **2017**, *6029–6034*, 6–11.

[24] B. Dereka, A. Rosspeintner, M. Krzeszewski, D. T. Gryko, E. Vauthey, *Angew. Chemie - Int. Ed.* **2016**, *55*, 15624–15628.

[25] W. Kim, J. Sung, M. Grzybowski, D. T. Gryko, D. Kim, *J. Phys. Chem. Lett.* **2016**, *7*, 3060–3066.

[26] T. Kim, J. Kim, H. Mori, S. Park, M. Lim, A. Osuka, D. Kim, *Phys. Chem. Chem. Phys.* **2017**, *19*, 13970–13977.

[27] T. Kim, W. Kim, H. Mori, A. Osuka, D. Kim, *J. Phys. Chem. C* **2018**, *122*, 19409–19415.

[28] F. Terenziani, A. Painelli, C. Katan, M. Charlot, M. Blanchard-Desce, *J. Am. Chem. Soc.* **2006**, *128*, 15742–15755.

[29] A. Janiga, E. Glodkowska-Mrowka, T. Stoklosa, D. T. Gryko, *Asian J. Org. Chem.* **2013**, *2*, 411–415.

[30] M. Krzeszewski, B. Thorsted, J. Brewer, D. T. Gryko, *J. Org. Chem.* **2014**, *79*, 3119–3128.

[31] Ł. G. Łukasiewicz, H. G. Ryu, A. Mikhaylov, C. Azarias, M. Banasiewicz, B. Kozankiewicz, K. H. Ahn, D. Jacquemin, A. Rebane, D. T. Gryko, *Chem. - An Asian J.* **2017**, *12*, 1736–1748.

[32] D. H. Friese, A. Mikhaylov, M. Krzeszewski, Y. M. Poronik, A. Rebane, K. Ruud, D. T. Gryko, *Chem. Eur. J.* **2015**, *21*, 18364–18374.

[33] M. Tasior, K. Hassanein, M. M. Leszek, I. Sakellari, D. Gray, M. Farsari, M. Samoc, F. Santoro, B. Ventura, D. T. Gryko, *Phys. Chem. Chem. Phys.* **2018**, 22260–22271.

[34] K. Oki, M. Takase, S. Mori, A. Shiotari, Y. Sugimoto, K. Ohara, T. Okujima, H. Uno, *J. Am. Chem. Soc.* **2018**, *140*, 10430–10434.

[35] H. Yokoi, Y. Hiraoka, S. Hiroto, D. Sakamaki, S. Seki, H. Shinokubo, *Nat. Commun.* **2015**, *6*, 8215–8223.

[36] D. Myśliwiec, M. Stępień, *Angew. Chemie - Int. Ed.* **2013**, 1713–1717.

[37] V. Weisskopf, E. Wigner, *Zeitschrift für Phys.* **1930**, 54–73.

[38] P. Meystre, M. Sargent, in *Elem. Quantum Opt., Springer Berlin Heidelberg, Berlin, Heidelberg*, **2007**, pp. 51–91.

[39] J. R. Lakowicz, *Principles of Fluorescence Spectroscopy*, Springer, New York, USA, **2006**.

[40] B. Valeur, *Molecular Fluorescence. Principles and Applications*, Wiley-VCH Verlag GmbH, **2001**.

[41] E. Runge, E. K. U. Gross, *Phys. Rev. Lett.* **1984**, *52*, 997–1000.

[42] R. Bauernschmitt, R. Ahlrichs, *Chem. Phys. Lett.* **1996**, *256*, 454–464.

[43] M. E. Casida, C. Jamorski, K. C. Casida, D. R. Salahub, *J. Chem. Phys.* **1998**, *108*, 4439–4449.

[44] D. Jacquemin, C. Adamo, *Chem. Soc. Rev.* **2013**, *42*, 845–856.

[45] J. Tomasi, B. Mennucci, R. Cammi, *Chem. Rev.* **2005**, *8*, 2999–3094.

[46] R. Cammi, S. Corni, B. Mennucci, J. Tomasi, *J. Chem. Phys.* **2005**, *122*, 104513.

[47] G. Scalmani, M. J. Frisch, B. Mennucci, J. Tomasi, R. Cammi, V. Barone, *J. Chem. Phys.* **2006**, *124*, 094107.

[48] A. D. Becke, *J. Chem. Phys.* **1993**, *98*, 5648.

[49] R. Improta, G. Scalmani, M. J. Frisch, V. Barone, *J. Chem. Phys.* **2007**, *127*, 074504.

[50] Z. L. Cai, K. Sendt, J. R. Reimers, *J. Chem. Phys.* **2002**, *117*, 5543–5549.

[51] A. Dreuw, M. Head-Gordon, *J. Am. Chem. Soc.* **2004**, *126*, 4007–4016.

[52] T. Yanai, D. P. Tew, N. C. Handy, *Chem. Phys. Lett.* **2004**, *393*, 51–57.

[53] F. L. Hirshfeld, *Theor. Chem. Acc.* **1977**, *44*, 129–138.

[54] A. Painelli, F. Terenziani, *J. Phys. Chem. A* **2000**, *104*, 11041–11048.

[55] B. Boldrini, E. Cavalli, A. Painelli, F. Terenziani, *J. Phys. Chem. A* **2002**, *106*, 6286–6294.

[56] C. Sissa, V. Parthasarathy, D. Drouin-Kucma, M. H. V Werts, M. Blanchard-Desce, F. Terenziani, *Phys. Chem. Chem. Phys.* **2010**, *12*, 11715–11727.

[57] F. Terenziani, A. Painelli, *Phys. Rev. B* **2003**, *68*, 165405–165413.

[58] G. D'Avino, F. Terenziani, A. Painelli, *J. Phys. Chem. B* **2006**, *110*, 25590–25592.

[59] C. Sissa, F. Terenziani, A. Painelli, A. Abbotto, L. Bellotto, C. Marinzi, E. Garbin, C. Ferrante, R. Bozio, *J. Phys. Chem. B* **2010**, *114*, 882–893.

[60] S. Sanyal, A. Painelli, S. K. Pati, F. Terenziani, C. Sissa, *Phys. Chem. Chem. Phys.* **2016**, *18*, 28198–28208.

[61] B. Bardi, C. Dall'Agnese, K. I. Moineau-Chane Ching, A. Painelli, F. Terenziani, *J. Phys. Chem. C* **2017**, *121*, 17466–17478.

[62] F. Terenziani, C. Sissa, A. Painelli, *J. Phys. Chem. B* **2008**, *112*, 5079–5087.

[63] F. Terenziani, O. V. Przhonska, S. Webster, L. A. Padilha, Y. L. Slominsky, I. G. Davydenko, A. O. Gerasov, Y. P. Kovtun, M. P. Shandura, A. D. Kachkovski, et al., *J. Phys. Chem. Lett.* **2010**, *1*, 1800–1804.

[64] A. Painelli, *Chem. Phys. Lett.* **1998**, *285*, 352–358.

[65] L. Onsager, *J. Am. Chem. Soc.* **1936**, *58*, 1486–1493.

[66] A. Painelli, F. Terenziani, *Chem. Phys. Lett.* **1999**, *312*, 211–220.

[67] M. J. Frisch, G. W. Trucks, H. B. Schlegel, G. E. Scuseria, M. A. Robb, J. R. Cheeseman, G. Scalmani, V. Barone, G. A. Petersson, H. Nakatsuji, et al., Gaussian 16, Revision B.01, Gaussian, Inc., Wallingford CT, **2016**.

Entry for the Table of Contents

Layout 1:

FULL PAPER

Emission solvatochromism of a centrosymmetric double helical π-expanded pyrrolo[3,2-*b*]pyrrole is related to symmetry breaking of the first excited state. Strong emission from the charge-transfer state is interpreted as borrowing intensity from the close-lying localized transitions, thus explaining the high and stable fluorescence quantum yield.

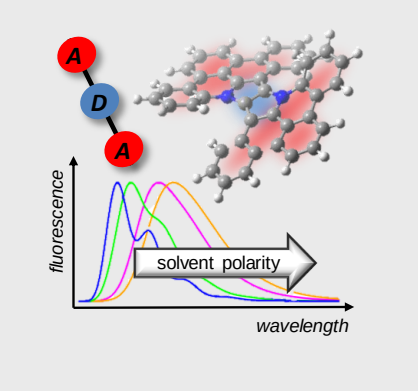

Brunella Bardi, Maciej Krzeszewski, Daniel T. Gryko, Anna Painelli, and Francesca Terenziani**

Page No. – Page No.

Excited-State Symmetry Breaking in an Aza-nanographene Dye